Rotational superstructure in van der Waals heterostructure of self-assembled C60 monolayer on the WSe2 surface

Rotational Superstructure in van der Waals Heterostructure of Self-Assembled C_{60} Monolayer on the WSe_2 Surface

Elton J. G. Santos,*,† Declan Scullion,† Ximo S. Chu,‡ Duo O. Li,‡ Nathan P. Guisinger,¶ and Qing Hua Wang*,‡

School of Mathematics and Physics, Queen's University Belfast, BT7 1NN, UK, Materials Science and Engineering, School for Engineering of Matter, Transport and Energy, Arizona State University, Tempe, Arizona 85287, USA, and Center for Nanoscale Materials, Argonne National Laboratory, Argonne, IL 60439, USA

E-mail: e.santos@qub.ac.uk; qhwang@asu.edu

*To whom correspondence should be addressed

†School of Mathematics and Physics, Queen's University Belfast, BT7 1NN, UK

‡Materials Science and Engineering, School for Engineering of Matter, Transport and Energy, Arizona State University, Tempe, Arizona 85287, USA

¶Center for Nanoscale Materials, Argonne National Laboratory, Argonne, IL 60439, USA

Abstract

Hybrid van der Waals (vdW) heterostructures composed of two-dimensional (2D) layered materials and self-assembled organic molecules are promising systems for electronic and optoelectronic applications with enhanced properties and performance. Control of molecular assembly is therefore paramount to fundamentally understand the nucleation, ordering, alignment, and electronic interaction of organic molecules with 2D materials. Here, we report the formation and detailed study of highly ordered, crystalline monolayers of C_{60} molecules self-assembled on the surface of WSe_2 in well-ordered arrays with large grain sizes ($\sim$5 μm). Using high-resolution scanning tunneling microscopy (STM), we observe a periodic 2×2 superstructure in the C_{60} monolayer and identify four distinct molecular appearances. Using vdW-corrected *ab initio* density functional theory (DFT) simulations, we determine that the interplay between vdW and Coulomb interactions as well as adsorbate–adsorbate and adsorbate–substrate interactions results in specific rotational arrangements of the molecules forming the superstructure. The orbital ordering through the relative positions of bonds in adjacent molecules create a charge redistribution that links the molecule units in a long-range network. This rotational superstructure extends throughout the self-assembled monolayer and opens a pathway towards engineering aligned hybrid organic/inorganic vdW heterostructures with 2D layered materials in a precise and controlled way.

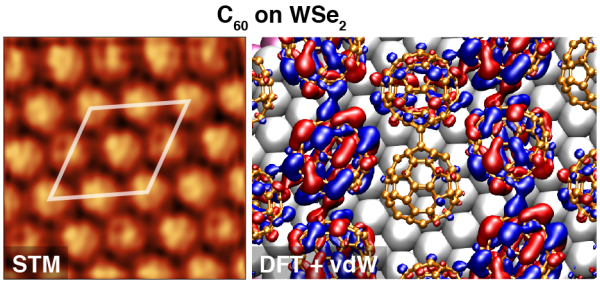

Graphical abstract

Keywords self-assembly, C_{60}, two-dimensional materials, scanning tunneling microscopy, density functional theory

Introduction

The intense development of two-dimensional (2D) materials in recent years has expanded into the study of heterostructures formed using 2D layers and other materials.[1–4] Heterostructures of different materials held together by van der Waals (vdW) forces allow materials of diverse compositions, structures, and properties to be combined, resulting in engineered materials with properties that are combinations of the components' properties, as well as newly emergent behaviours at the interfaces. Such heterostructures have been demonstrated using stacks of 2D layered materials[1–4] and 2D materials combined with nanostructures of other dimensionalities and with organic crystals.[5] The atomic flatness and lack of dangling bonds at the surface of 2D layered materials like graphene, boron nitride, and the transition metal dichalcogenides (TMDCs) allow them to form non-covalent interactions with a wide range of materials without the requirements for lattice matching that covalently bonded systems would have. Heterostructures of 2D layers can be achieved by physically stacking different sheets together or by epitaxial growth of subsequent 2D materials.[1–4,6,7] At the interfaces between disparate materials, effects like charge transfer, tunneling, disorder, and impurity states can influence the electronic and optical behaviours.[8] The careful combination of materials has resulted in new developments in performance and properties in devices like transistors, solar cells, and light emitting diodes.[5,9,10]

The vdW heterostructures formed by organic crystals on 2D layered materials generally take advantage of the atomically flat and chemically inert surfaces to template self-assembly of the molecule units into ordered arrangements.[5,11–17] Organic molecules that are often used in organic electronics, which typically have conjugated $\pi-$electron systems for better intermolecular conduction,[18] have improved stacking and ordering when they are assembled by 2D materials.[16] This has resulted in devices with significant increases in carrier mobility in field-effect transistors[5,19,20] and increased charge separation in photovoltaics.[21] There are also promising opportunities for organic/2D vdW heterostructures to be used in flexible

electronics.[22–24] The synergy between the mechanical robustness of the 2D layers and their diverse available electronic properties, ranging from semi-metals (e.g. graphene, silicene, germanene) to semiconductors (e.g. transition metal dichalcogenides (TMDCs)),[25] combined with the chemical tunability of the molecules can open the door for further design rules based on organic/vdW heterostructures. There is a need to develop a fundamental understanding of how molecular processes happening at the early stage of the crystallization of organic molecules on 2D crystals drive the system to specific epitaxial relationships[11] and unique interfacial properties such as polymorphism.[12] Moreover, the control of two-dimensional self-assembly of single-layer of molecules on layered materials in terms of molecular ordering, alignment, and crystallinity can result in emergent behavior and exciting new physics. Therefore, it is essential to achieve a deep understanding of the basic physical and chemical phenomena that rule highly crystalline architectures involving crystals of organic molecules and 2D materials in potential device platforms.

Here we report the growth of high quality self-assembled monolayers of C_{60} on WSe_2 as an example of a weakly interacting organic/2D vdW heterostructure system. C_{60} has been extensively used in the organic electronics field, and WSe_2 is an important semiconducting 2D material. We study the interfacial properties of this system using complementary methods of high resolution scanning tunneling microscopy (STM) and *ab initio* density functional theory including vdW interactions. C_{60} plays an important role as an acceptor in organic photovoltaics (OPVs)[26,27] due to its high electron affinity for charge harvesting processes, and is expected to be similarly useful in hybrid 2D/organic optoelectronics.[28] The interfacial interaction of C_{60} with other 2D TMDCs has been shown to result in doping, with p-doping occurring for WSe_2 in particular,[29] and with graphene has led to charge transfer and increased carrier mobility.[30] While the self-assembly of C_{60} molecules on metal surfaces like Cu,[31–34] Au,[32,35–42] and Ag[32,35,40] has been widely studied by STM, their behavior on 2D material substrates is relatively unknown aside from some studies on graphene.[15,43–46] The electronic and physical structure of the substrate has played an important role in these

earlier works, and is also expected to be crucial in the case of WSe_2. Generally, there is a higher degree of charge transfer between metals and molecules than between 2D materials and molecules.

Our STM images reveal that C_{60} self-assembles into a close-packed monolayer on the surface of WSe_2 that extends uniformly in islands as large as $\sim$5 μm. The long-range ordering and large grains we observe contrast with much smaller grains and local ordering seen in previous studies. This C_{60} monolayer exhibits four distinct intramolecular patterns in a 2×2 superlattice, which is unusual for a monolayer assembly. High-throughput first-principles calculations show that only a few molecular configurations are energetically favorable for C_{60} arranged on WSe_2. The relative orientation of pentagons and hexagons between neighboring molecules drives the different arrangements through charge reordering connecting the C_{60} molecules in a periodic network. Moreover, a systematic increase of the charge transfer between WSe_2 and C_{60} is observed as a function of short rotations of C_{60} mediated by vdW interactions. The increase in electron transfer goes along with the increase in stability of molecular configuration. This observation points to the active role of the molecule–substrate interactions in the stabilization of the interface. This also indicates that the presence of C_{60} has only a mild effect on the physical and electronic properties of WSe_2 (e.g. electronic band gap, W-Se bond length, flatness), even though the molecules are electronically correlated. The creation of a clean interface between WSe_2 and C_{60} resulting in a unique rotational superlattice is an intriguing step in the understanding and engineering of organic/2D vdW heterojunction devices.

Results and discussion

Formation of self-assembled C_{60} monolayer

The assembly of C_{60} on WSe_2 was experimentally implemented by *in situ* thermal deposition of C_{60} in an ultrahigh vacuum (UHV) system and characterized by scanning tunneling

microscopy (STM). A single-crystal WSe_2 substrate was cleaved by scotch tape to expose a clean surface immediately before being introduced into the vacuum chamber for characterization and thermal deposition of C_{60}. STM images of the clean WSe_2 surface are shown in Fig. 1**a**-**b**. The atomic structure of the WSe_2 lattice is clearly visible in both images, with a triangular symmetry due to the alternating positions of the Se atoms at the surface. Two point defects are seen in Fig. 1**a**, and some undulation of the surface in Fig. 1**b**. Fullerene molecules (C_{60}) were thermally evaporated in situ onto the WSe_2 surface held at room temperature. The deposition time was calibrated such that we achieved sub-monolayer coverage of C_{60} molecules. A schematic illustration of the C_{60} molecules on top of WSe_2 is shown in Fig. 1**c**.

The sample was then cooled to 55 K for STM imaging, which showed that the fullerenes self-assemble into a close-packed hexagonal layer on WSe_2, as seen in Fig. 1**d**. Because the sample is well below room temperature, the thermal motion of the molecules is minimized so that they can form a stable island with clear boundaries and long-range ordering. We note that bulk C_{60} crystals, which pack in a face-centered cubic (fcc) lattice, have fewer rotational freedoms below 260 K, and have their orientational alignments frozen below 90 K.[47,48] In our experiments, the substrate is at room temperature during thermal deposition of C_{60}, allowing sufficient energy for the molecules to rotate and interact. The entire C_{60}/WSe_2 system is then gradually cooled to 55 K, so that the optimal molecular configurations are stabilized before STM imaging.

The apparent height of the molecules is about 1 nm, as shown in the line profile labeled '1'. This height is similar to that of a C_{60} monolayer grown on NaCl crystals on Au(111), and is higher than the $\sim$0.6-0.7 nm observed for C_{60} on Au(111).[38] The inset of Fig. 1**d** shows a 2D fast Fourier transform (FFT) of the C_{60} region, with sharp points in a hexagonal pattern. The distance from the center to each point is approximately 1.0 nm^{-1}, corresponding to a periodicity of approximately 1.0 nm between molecules. This close-packed arrangement of the C_{60} on WSe_2 is similar to its arrangement on other substrates such as graphene,[15,49]

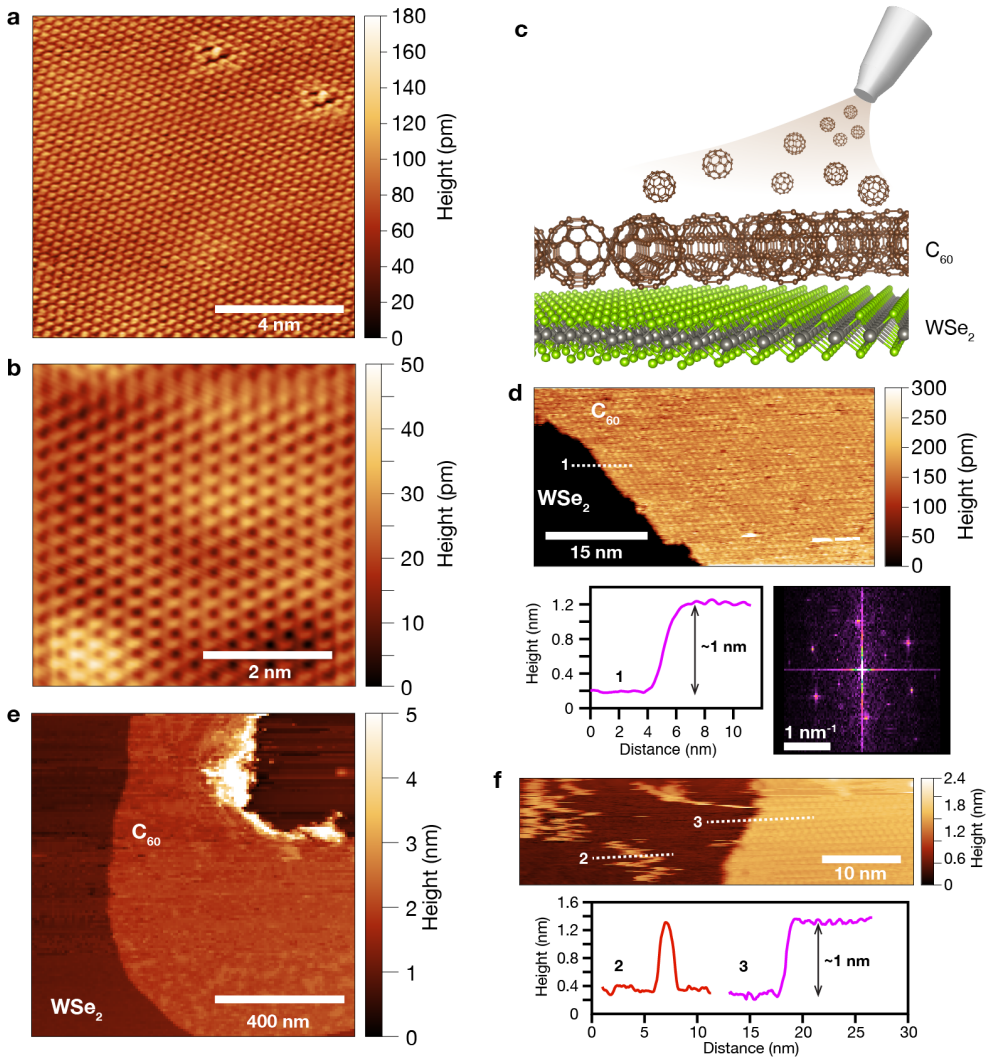

Figure 1: Self-assembly of C_{60} on WSe_2. (**a**)-(**b**) Scanning tunneling microscopy (STM) images of mechanically exfoliated WSe_2. The atomic lattice is visible in both images, along with two point defects in (a) and some local height variations in (b). Imaging conditions for (a) and (b): 0.6 V sample bias, 1 nA tunneling current setpoint, 55 K sample temperature. (**c**) Schematic illustration of monolayer of C_{60} deposited by thermal evaporation and self-assembled on WSe_2 surface. (**d**) STM image of C_{60} self-assembled monolayer island on WSe_2. The flat WSe_2 surface at the lower left of image appears very dark because the height scale has been adjusted to show periodicity in the C_{60} molecules. Below: Line profile along dashed line 1, showing height of C_{60} molecules is 1 nm, and 2D FFT of the C_{60} molecular arrangement, showing the points corresponding to a hexagonal pattern. Imaging conditions for (d): 2.5 V sample bias, 0.1 nA tunneling current setpoint, 55 K sample temperature. (**e**) STM image showing larger area of C_{60} island on WSe_2. Imaging conditions: 3.0 V sample bias, 0.1 nA tunneling current. (**f**) STM image of the edge of a submonolayer island of C_{60}, showing some molecules moving away from the edge at the left. The heights of the loose molecules and the rest of the island are the same, suggesting that the observed orderly arrangements are monolayers rather than bilayers. Imaging conditions: 2.2 V sample bias, 0.05 nA tunneling current.

Au,[41,42] and Cu.[46] It is also similar to the (111) cut through the bulk fcc C_{60} crystal. In contrast, on reactive surfaces with dangling bonds such as Si and SiC, C_{60} forms covalent bonds with the surface and do not form well-ordered layers,[50–52] although multilayers of C_{60} can form ordered lattices.[53]

We observe large islands of C_{60} (Fig. 1**e**) with dimensions up to $\sim$5 μm. In contrast, molecular islands of C_{60} on other substrates in the literature tend to be less than 100 nm in diameter.[15,38,46] We observe some instances of molecules freely moving across the WSe_2 surface with the same apparent 1 nm height, such as the ones in the line profile labeled '2' in Fig. 1**f**, confirming that our molecular islands are indeed monolayers of C_{60} rather than bilayers. Line profile '3' is taken at the edge of a molecular island.

In the high-resolution STM images of Fig. 2, the individual C_{60} molecules appear to have submolecular structure, relating to the complex shape of the electronic orbitals in the molecule. The distance between adjacent C_{60} molecules is approximately 1.0 nm (see line profile in Supporting Information, Figure S3). We can identify four individual configurations of C_{60}, as highlighted by the circles labeled i, ii, iii, and iv in Fig. 2**a**. Each of these molecules is enlarged and cropped in Fig. 2**b** to more clearly show their distinct appearances. Since sample bias is +2.0 V in these images, these orbitals are likely to correspond to empty states (lowest unoccupied molecular orbitals, LUMO).

To understand the variations of the appearance of each C_{60} molecule on WSe_2, we have performed first-principles density functional theory (DFT) calculations taking into consideration van der Waals (vdW) dispersion forces (see Methods section and Supplementary Information for details). As described below in detail, we can identify the most likely interface geometry as indicated in each simulated STM image in Fig. 2**b**. We have simulated the STM images for more than ten different configurations of C_{60} on top of WSe_2 (see Fig. S1 in Supplementary Materials), with their energies shown in Fig. 3 as discussed in more detail below. These configurations can be organized in three different sets of symmetries as described in terms of observed rotational symmetry of the orbital lobes, e.g. 2-, 3- and 5-fold. Each

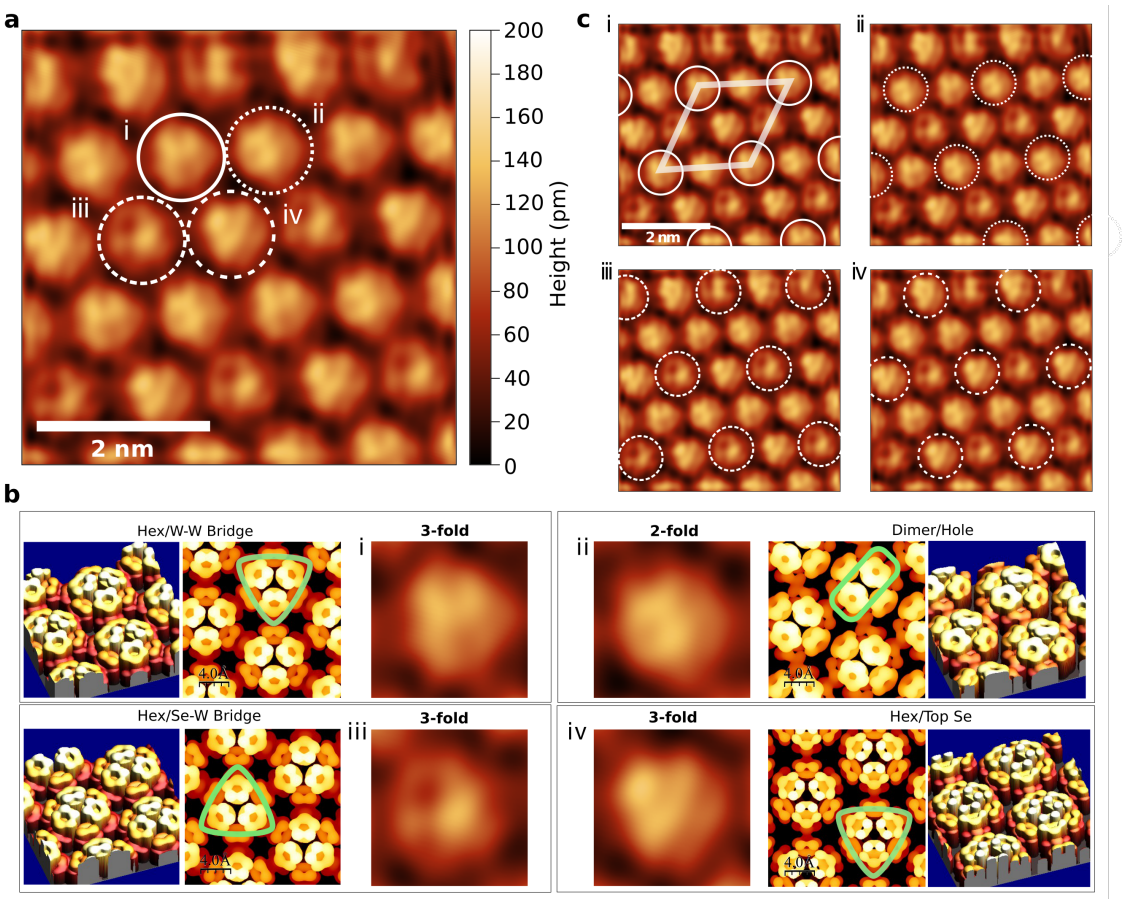

Figure 2: Molecular orientation superlattice of C_{60} on WSe_2. (**a**) STM image of self-assembled monolayer of C_{60} molecules with submolecular resolution showing shapes of orbitals. Since the sample bias is +2.0 V, these are likely empty states (LUMO). The molecules are in a close-packed hexagonal arrangement. Four different orbital appearances are highlighted in the different circles, labeled i, ii, iii, iv, and are potentially attributed to different molecular orientations on the substrate surface. (**b**) Enlarged and cropped images of the four circled molecules from panel (a), showing their distinct appearances. Simulated STM images in 2D and 3D views are shown beside each panel with the corresponding interface geometries. The dominant symmetry (2-, 3-fold) at each image is highlighted with green-outlines on the simulations. (**c**) The STM image from panel (a) is repeated here, with each of the four orbital appearances highlighted. They form a 2×2 superlattice arrangement as marked in panel i. Imaging conditions: 2.0 V sample bias, 0.2 nA tunneling current setpoint, 55 K sample temperature.

interfacial molecule seems to follow these symmetry rules even at the limit of full surface coverage. Indeed, looking closely at this limit we notice that these orbital appearances also form a 2×2 superlattice, as highlighted in Fig. 2**c**. Each of the appearances i-iv is highlighted in each panel, with the circles indicating the repeated molecules. It is clear that each molecular appearance arises in the self-assembled monolayer of C_{60} every two molecules (Fig. 2**c**, panel i) to form a hexagonal pattern. In this 2×2 superlattice the distance between nearest neighboring molecules is 9.89 Å, which is close to the vdW distance in C_{60} bulk crystals.[54] We emphasize here that this 2×2 superlattice is observed in a monolayer of C_{60}, while previous reports of orientational superlattices in C_{60} have been in bilayers on Au(111),[42] multilayers on Cu(111),[55] bulk C_{60} crystals,[53] multilayers on Ag(111) with some local ordering,[56] and bilayers and multilayers on NaCl/Au(111).[38] There have also been superstructures observed by STM for C_{60} on epitaxial graphene due to electronic Moiré patterns with either the Ru(0001) or SiC(0001) substrates rather than due to molecular rotations.[15,43]

Configurations and rotations of C_{60} on WSe_2

To determine the effect of the interactions on the observed molecular patterns, we used *ab initio* calculations at two different levels of theory with van der Waals interactions (DRSLL functional) and without (GGA, PBE functional). (See Methods section below and Supplementary Information for details.) We have initially considered a number of C_{60} molecular configurations on the WSe_2 surface and calculated their electronic and energetic structures for a freestanding layer. A computational high-throughput screening taking into account the orientation of C atoms in the C_{60} molecule in pentagon, hexagon, dimer and apex positions, relative to the WSe_2 structure, resulted in sixteen different arrangements as shown in Fig. 3. We clearly observed the role of vdW dispersion forces in the stabilization of the C_{60}/WSe_2 interfaces as we compare Fig. 3**a** and 3**b**. There is an enhancement of the stability in the vdW simulations as high as one order of magnitude relative to GGA results. The energy difference between the lowest and the highest stable configurations reaches 0.10 eV and 0.30 eV

in GGA and vdW, respectively. We also observed that this increase in stability among the different configurations originates as C_{60} molecules partially rotate on the WSe_2 surface, with the most stable configuration being the one where a hexagonal ring is on top of a Se atom (Hexagon/Top Se, top right of Fig. 3). This effect also influences the amount of charge transferred from WSe_2 towards C_{60}, which follows the vdW stability. As the interactions increase with more stability, the molecular orbitals of the C_{60} overlap more with the states at the surface, which increases the amount of charge transfer towards C_{60}. That is, the more stable the configuration the more electron transfer. This is in accordance with the good acceptor characteristics of C_{60} due to its high electron affinity, which is advantageous in organic solar cells.[57,58] This also agrees with the spectroscopic observation of C_{60} causing p-doping in WSe_2.[29]

We now address the different relative orientations between the molecules in the 2×2 superlattice measured above (Fig. 2). It is well established that C_{60} molecules tend to perform rotations along some preferential directions when physisorbed on top of weakly interacting surfaces.[59–65] The strength of molecule–surface interactions and molecule–molecule forces determine the angular orientations of C_{60}, which can vary as a function of temperature. When C_{60} is deposited on WSe_2 surfaces, the molecules will have enough energy to perform molecular spinning, translations and some vibrations, e.g. breathing modes, as simulated using *ab initio* molecular dynamics at 55 K and 355 K (see Fig. 4, and movies in Supplementary Information). Most of the molecules perform short rotations in the first 1.0 ps, assuming different configurations relative to each other at later times. A constant spinning rate of all molecules has not been observed simultaneously for any initial configuration. Fig. 4**a** shows the initial and final configurations after the system has time evolved for 10.5 ps. The relative positions of the atoms of the C_{60} molecules are highlighted in blue and yellow to follow the evolution with time of the hexagonal and pentagonal rings, respectively, in each molecule. Interestingly, the molecular dynamics indicates that some molecules have their movement coupled to the nearest neighbors through interactions of double bonds localized between two

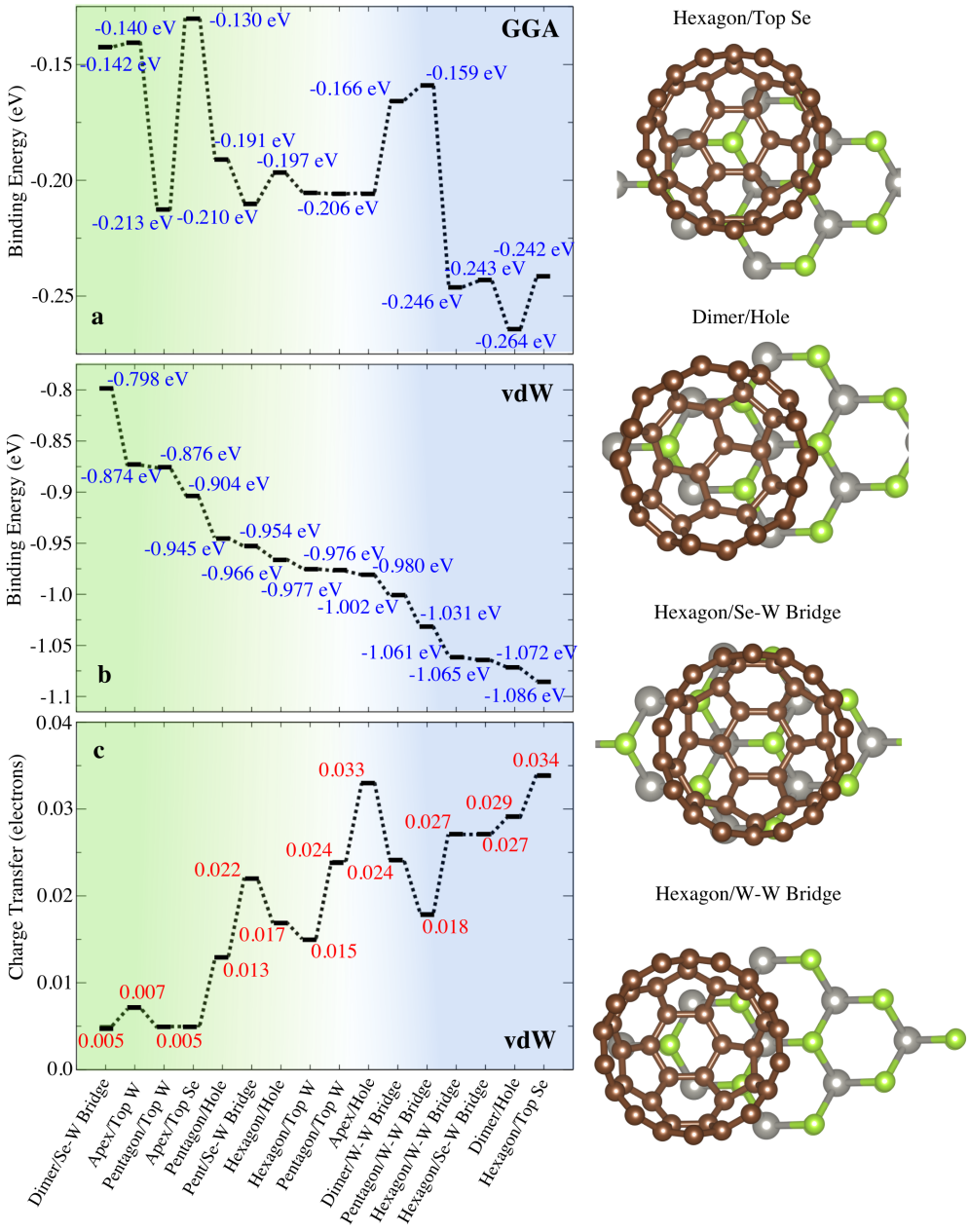

Figure 3: *ab initio* **vdW electronic structure calculations.** (**a**),(**b**) Calculated binding energies per C_{60} molecule at the level of GGA (PBE) and vdW (DRSLL) density functional theory, respectively, for a high-throughput computation screening of several configurations between C_{60} and WSe_2. Configurations are ordered from the lowest to the highest bindings based on the vdW energy results. The four most stable molecular interfaces are shown on the right side in a top view perspective named accordingly to relative configuration of the C (brown), Mo (gray) and Se (green) atoms. For instance, a hexagonal ring in C_{60} might face the WSe_2 surface in different ways, such as standing on top of a Se atom (Hexagon/Top Se), or at a Se-W bridge position (Hexagon/Se-W bridge). (**c**) Interfacial charge transfer per molecule calculated at the level of vdW from WSe_2 towards C_{60}.

hexagons (6:6) on one molecule and pentagonal faces of an adjacent C_{60} molecule (see movie 1 in Supplementary Materials). Such 6:6 bonds have a higher electronic density than bonds localized between a hexagon and pentagon (6:5) because of the local aromatic character.[54,66] This serves as an efficient point of interactions between the molecules.

Electronic structure of hybrid C_{60} / WSe_2 system

The energetic barriers for rotation between adjacent C_{60} molecules as a function of rotation angle θ (Fig. 4**b**) show that the most stable positions occur at 0^o and 60^o, which are angles where a 6:6 bond faces a pentagon (Fig. 4**c**). In this situation the high charge density of p_z orbitals in 6:6 bonds overlap electron-poor pentagonal zones, which minimizes Coulomb interactions between molecules, therefore reducing the total energy of the system. The tendency for electron-rich and electron-poor regions of adjacent C_{60} molecules to associate has been also seen in previous reports.[38] The wavefunctions of the conduction band at different rotational angles θ show the different orbital overlaps between the molecules (Fig. 4**d-e**). In all configurations a substantial interaction is observed, with $\theta = 30^\circ$ corresponding to two 6:6 bonds facing each other as the strongest (Fig. 4**e**). This configuration raises the energy by $\sim$334 meV (Fig. 4**b**), but provided an efficient coupling between C_{60} molecules as observed in the substantial charge density present throughout the entire system. Repulsive forces based on the short-range Pauli exclusion regime drive the system to short rotations where the strong overlap in wavefunctions between adjacent molecules can be tuned. It is noted that the charge density localized in the inter-molecule space clearly modifies its shape at different values of θ, being more orbital-localized at low interactions energies (Fig. 4**d**), rather than spread between different molecules at high energy cost (Fig. 4**e**).

Furthermore, some meta-stable positions are also observed around $\theta = 15^\circ$ and $\theta = 45^\circ$, which are due to the stabilization of the charge arrangement between different C_{60} bonds; that is, 6:5 bonds and apex atoms in the C_{60}. This suggests the directional nature of the C_{60}–C_{60} interactions in the monolayer which acts as a driving force for organization and

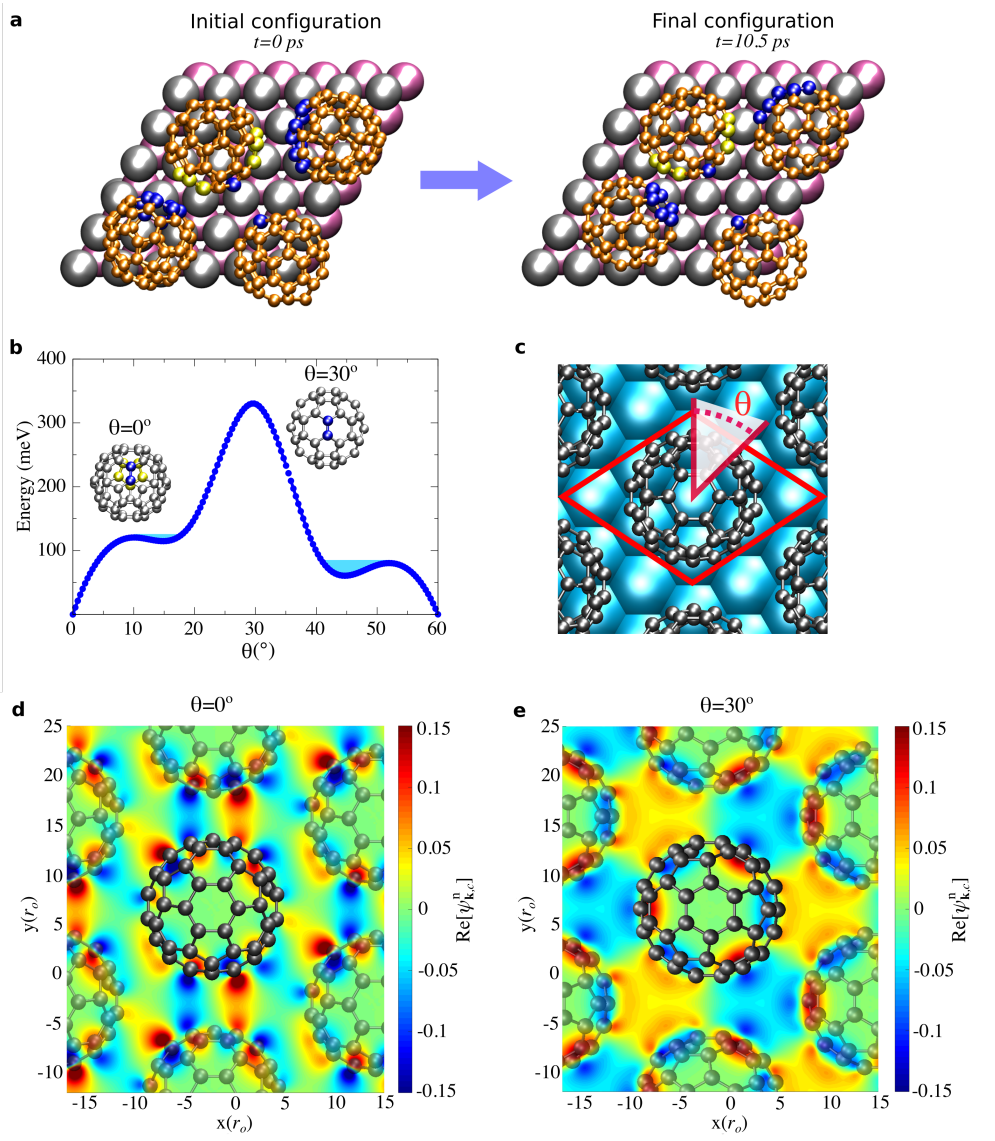

Figure 4: Molecular coupling in C_{60} molecules. (**a**) *Ab initio* molecular dynamics simulations including vdW dispersion forces for C_{60} molecules on WSe_2. Atoms highlighted in blue (involving hexagons) and yellow (involving pentagons) tracked down the evolution of the molecules during the molecular dynamics where most of the interactions between the molecules happen. The system is set at $T = 355$ K, and time-evolved for $t = 10.5$ ps. (**b**) Rotational barriers per interfacial molecule for C_{60} at the most stable configuration of Fig.3**b** (Hexagon/Top Se). (**c**) Schematic of the unit cell and the definition of the rotational angle θ utilized in **b** relative to the next-neighbor molecules. The rotational angle θ is defined relative to the equator of the C_{60} molecule where spinning occurs along its center. Different angles correspond to distinct relative orientations between the C_{60}'s: $\theta = 0^{\circ}$ (pentagon/6:6 configuration), $\theta = 10^{\circ}$ (6:5/6:5 configuration), $\theta = 30^{\circ}$ (6:6/6:6 configuration). Similar orientations are observed for $\theta > 30$ because of the 3-fold symmetry. (**d-e**) Cross section of the real part of the wave functions corresponding to the bottom of the conduction band $\psi^{n}_{\mathbf{k},c}$ at $\theta = 0^{\circ}$ and $\theta = 30^{\circ}$, respectively. Positive and negative values are shown in the color gradient map at the right of each panel. C atoms are shown in dark gray.

self-assembly. Indeed, an estimation of the molecule–molecule interactions in the periodic two-dimensional C_{60} monolayer without the WSe_2 gives a binding energy of 0.70 eV ($\theta = 0$), which is slightly smaller than those calculated between substrate and molecule at different adsorption configurations (Fig.3**b**) but still in the same energy range. This indicates that some competition between molecule–molecule and molecule–surface interactions takes place at different values of θ. In comparison to experiments performed on other surfaces,[42,55] where there are stronger interactions between C_{60} molecules and substrates, superlattices were only observed in bilayer islands likely due to the decoupling of the second layer from the substrate. In our experiments, the superlattice is observed in the C_{60} monolayer. If the balance between repulsion and attraction within the C_{60} monolayer is altered due to high molecule–surface interactions, similar patterns would not be observed. We emphasize that here in the case of WSe_2 surfaces, the interactions are at just the right amount to permit the C_{60} molecules to spin and still be chemically coupled to the substrate.

The resulting electronic structure of the combined C_{60}/WSe_2 system after 10.5 ps of time evolution is shown in Fig. 5. The geometric configuration of the system is the one shown in Fig. 4**a**. A band gap of about 0.50 eV is clearly observed in the C_{60}/WSe_2 system, with contributions from conduction band C_{60} states (Fig. 5**a**). The bandgap of the C_{60} layer alone is close to 0.7 eV, which is considerably smaller than that of C_{60} packed in an FCC solid and smaller than the HOMO-LUMO gap of the isolated molecule,[54] but is close to what was measured for C_{60} in a double barrier tunnel junction geometry.[67] This suggests that some delocalization of the C_{60} states throughout the entire system could be a key factor. Indeed, the real part of the fullerene wave functions, $\mathrm{Re}[\psi^{\mathrm{n}}_{\mathbf{k},c}]$ ($\mathrm{n} = 4, 7$), selected at the conduction band displayed such behavior (Fig. 5**b-c**). There is a remarkable electronic interaction between the C_{60} molecules which can be appreciated via the lateral extension of the molecular orbital linking the molecules in different spatial distributions. In fact, such orbital characteristics follow a molecular pattern that resembles the one observed in our STM measurements (Fig. 2). The spatial character of the wave function changes between

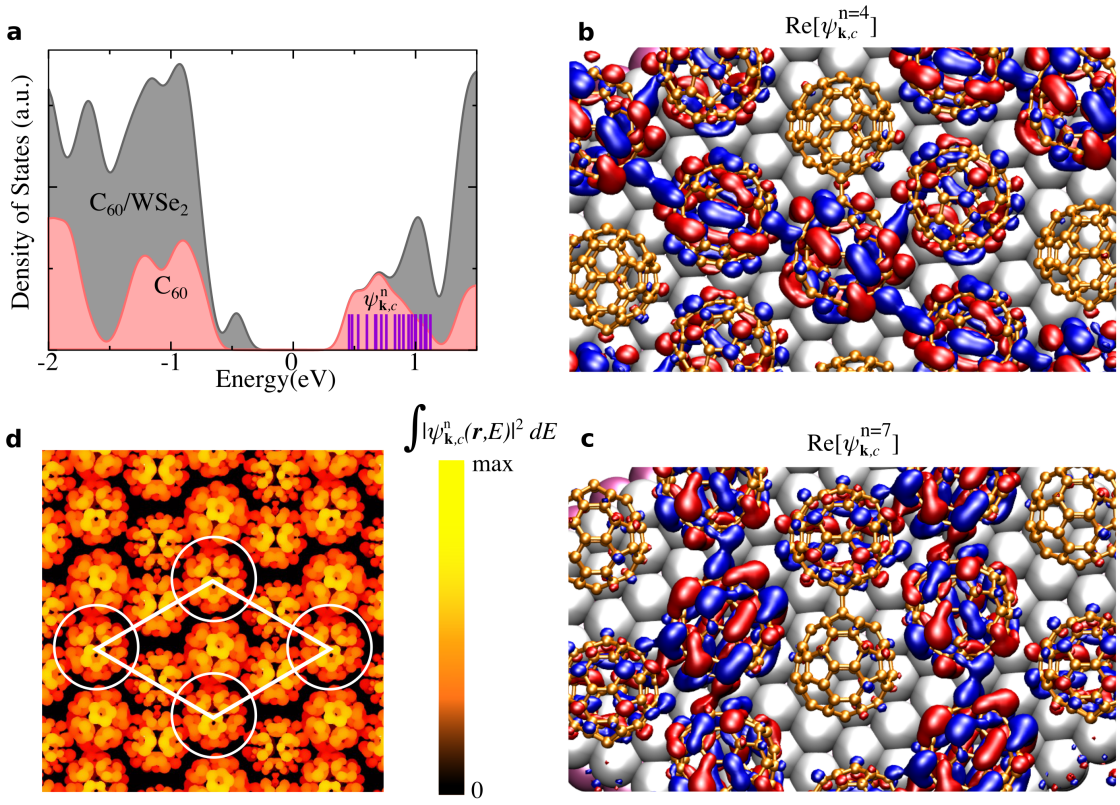

Figure 5: Electronic structure of C_{60}/WSe_2 heterostructure. (**a**) Density of states (DOS) of the C_{60}/WSe_2 heterostructure (gray) and C_{60} monolayer (pink) for the optimized geometry at 355 K using *ab initio* molecular dynamics simulations as shown in Fig. 4**a**. The states at the bottom of the conduction band are shown individually through vertical bars with $\psi^{n}_{\mathbf{k},c}$, where $n = 1-19$. Fermi level is set to zero. (**b-c**) Isosurfaces (± 0.001 e/Bohr^3) for the real part of the wave functions corresponding to the fourth and seventh eigenvalues, $\psi^{n=4,7}_{\mathbf{k},c}$ of the DOS represented in panel **a**. These eigenvalues are arbitrarily chosen to be representative ones from the full set of states at the conduction band. Most of the wave functions show similar interacting patterns between the molecules with slight variations between different $\psi^{n}_{\mathbf{k},c}$. Here we highlight only two of them, while other examples are shown in Fig. S2. Positive and negative parts of $\psi^{n}_{\mathbf{k},c}$ are shown in blue and red, respectively. Se, W and C atoms are shown in silver, pink and orange, respectively. (**d**) Local density of states plotted using the integration of all energy levels marked as $\psi^{n}_{\mathbf{k},c}$ ($n = 1-19$) in **a**. The periodicity of the 2×2 superlattice is highlighted for a particular C_{60} configuration in the supercell.

one eigenvalue to another, not only for n = 4, 7, but the orbital symmetry involved at each molecule is kept the same (see Fig. S2). In particular, all the eigenstates marked in Fig. 5**a** at the bottom of the conduction band in the range of 0.45 eV to 1.12 eV inside of the band gap of the WSe_2 surface have similar electronic characteristics. Integrating these states through:

$$\rho(\mathbf{r}, E) = \int_{E_o}^{E_o+\epsilon} |\psi^{\mathrm{n}}_{\mathbf{k},c}(\mathbf{r}, E)|^2 dE \tag{1}$$

gives their spatial distribution in terms of the local density of states as shown in Fig. 5**d**. The quantity $\rho(\mathbf{r}, E)$ reproduces closely the main features observed in the measured STM images (Fig. 2), where every other molecule has the same molecular orbital distribution following a 2×2 superlattice. The precise combination of the C_{60} molecules in the supercell utilized can drive the system to different orientationally ordered C_{60} domains. However, once the main interactions between molecules and molecule–substrate take place the rotational superstructure is formed, even though the local molecular configuration of the individual C_{60} molecules might show differences. This is related with the dynamical aspect of the molecule itself associated with the collective character of the self-assembly.

Conclusion

In conclusion, our findings reveal fundamental knowledge of the physical and chemical phenomena of van der Waals heterostructures using self-assembled organic molecules and inorganic 2D materials, which have some subtle but important differences from self-assembly on metal surfaces. C_{60}/WSe_2 constitutes an archetypal vdW heterostructure with exciting possibilities for electronic devices based on atomically thin films. We have shown the self-assembly of C_{60} molecules on WSe_2 layers via high-resolution STM and *ab initio* DFT including vdW interactions. After deposition, the molecules form a monolayer that extends uniformly over WSe_2 with large grain sizes (∼5 μm). The interplay and balance between

adsorbate–adsorbate and adsorbate–substrate interactions leads to the formation of rotational arrays of self-assembled 2×2 molecules. Using the state-of-the-art vdW *ab initio* calculations, we demonstrate the critical role of the relative orientation between specific bonds in the C_{60} in the determination of the spatial superlattice. Through the minimization of the inter-molecule Coulomb interactions, the C_{60} molecules tend to be electronically coupled with long range orientational ordering, which is reflected in the high crystallinity of C_{60} on WSe_2. The electronic structure of the hybrid system shows spatial delocalization of molecular orbitals throughout the 2×2 superlattice. The present study shows a mechanism of collective molecular restructuring based on the balance of non-covalent molecule–molecule and molecule–substrate interactions. These results may have implications in the geometrical control of the self-assembly of surface molecules for various electronic and optoelectronic applications based on vdW heterostructures of 2D materials. This highlights the advantages of organic vdW heterostructures over commonly used materials to achieve high-performance organic electronic devices, where such control of molecule assembly is not achievable. Future theoretical and experimental efforts will explore to what extent the surface-driven molecular self-assembly mechanism found here will influence the carrier mobility of the organic molecules, which is critical for device platforms.

Methods

Fabrication of the WSe_2/C_{60} heterostructure and measurements

Ultrahigh vacuum scanning tunneling microscopy (UHV STM) imaging was conducted in an Omicron VT STM/AFM system. The WSe_2 crystal (NanoScience Instruments) was cleaved by peeling away the top layer using adhesive tape in air, and then was immediately loaded into the vacuum system. The C_{60} molecules (Sigma Aldrich, sublimed, 99.9%) were deposited in vacuum using a molecular beam thermal evaporator (Dodecon Nanotechnology GmbH) onto the WSe_2 sample held at room temperature. STM probes were electrochemically etched

W wire. The WSe_2 sample with C_{60} monolayer was cooled to 55 K for all imaging. The STM electronics and software were from Nanonis, and the resulting images were processed with the Gwyddion software package.[68] Image processing included low-pass noise removal and background flattening.

vdW ab initio calculations

Calculations were based on *ab initio* density functional theory using the SIESTA method[69] and the VASP code.[70,71] The generalized gradient approximation[72] along with the DRSLL[73] functional was used in both methods, together with a double-zeta polarized basis set in SIESTA, and a well-converged plane-wave cutoff of 500 eV in VASP. We used a Fermi-Dirac distribution with an electronic temperature of $k_{BT} = 20$ meV. Additional details are provided in the Supporting Information.

Acknowledgments

Use of the Center for Nanoscale Materials, an Office of Science user facility, was supported by the U. S. Department of Energy, Office of Science, Office of Basic Energy Sciences, under Contract No. DE-AC02-06CH11357. E.J.G.S. acknowledges the use of computational resources from the UK national high performance computing service, ARCHER, for which access was obtained via the UKCP consortium and funded by EPSRC grant ref EP/K013564/1; and the Extreme Science and Engineering Discovery Environment (XSEDE), supported by NSF grants number TG-DMR120049 and TG-DMR150017. The Queen's Fellow Award through the startup grant number M8407MPH and the Energy Sustainable PRP (QUB) are also acknowledged. D.S. acknowledges the EPSRC studentship. Q.H.W. acknowledges support from Arizona State University startup funds.

Author Contributions

Q.H.W. and E.J.G.S. designed the project, analyzed the data, and wrote the manuscript. E.J.G.S. and D.S. conducted the DFT calculations. Q.H.W., N.P.G., X.S.C., and D.O.L. conducted the STM experiments.

Supporting Information

Supporting Information Available: Additional details on calculation methods, simulated STM images of all C_{60} configurations on WSe_2, wavefunctions of C_{60}/WSe_2, and molecular dynamics movies of C_{60} on WSe_2.

Notes

The authors declare no competing financial interest.

References

1. Geim, A. K.; Grigorieva, I. V. Van der Waals heterostructures. *Nature* **2013**, *499*, 419–425.

2. Lee, G.-H.; Yu, Y.-J.; Cui, X.; Petrone, N.; Lee, C.-H.; Choi, M. S.; Lee, D.-Y.; Lee, C.; Yoo, W. J.; Watanabe, K. et al. Flexible and Transparent MoS_2 Field-Effect Transistors on Hexagonal Boron Nitride-Graphene Heterostructures. *ACS Nano* **2013**, *7*, 7931–7936.

3. Liu, Y.; Weiss, N. O.; Duan, X.; Cheng, H.-C.; Huang, Y.; Duan, X. Van der Waals heterostructures and devices. *Nature Rev. Mater.* **2016**, *1*, 16042.

4. Novoselov, K. S.; Mishchenko, A.; Carvalho, A.; Castro Neto, A. H. 2D materials and van der Waals heterostructures. *Science* **2016**, *353*, aac9439.

5. Lee, C.-H.; Schiros, T.; Santos, E. J. G.; Kim, B.; Yager, K. G.; Kang, S. J.; Lee, S.; Yu, J.; Watanabe, K.; Taniguchi, T. et al. Epitaxial Growth of Molecular Crystals on

van der Waals Substrates for High-Performance Organic Electronics. *Adv. Mater.* **2014**, *26*, 2812–2817.

6. Withers, F.; Del Pozo-Zamudio, O.; Mishchenko, A.; Rooney, A. P.; Gholinia, A.; Watanabe, K.; Taniguchi, T.; Haigh, S. J.; Geim, A. K.; Tartakovskii, A. I. et al. Light-emitting diodes by band-structure engineering in van der Waals heterostructures. *Nature Mater.* **2015**, *14*, 301–306.

7. Jariwala, D.; Marks, T. J.; Hersam, M. C. Mixed-dimensional van der Waals heterostructures. *Nature Mater.* **2017**, *16*, 170–181.

8. Li, S.-L.; Tsukagoshi, K.; Orgiu, E.; Samori, P. Charge transport and mobility engineering in two-dimensional transition metal chalcogenide semiconductors. *Chem. Soc. Rev.* **2016**, *45*, 118–151.

9. Jeong, H.; Bang, S.; Oh, H. M.; Jeong, H. J.; An, S.-J.; Han, G. H.; Kim, H.; Kim, K. K.; Park, J. C.; Lee, Y. H. et al. Semiconductor-Insulator-Semiconductor Diode Consisting of Monolayer MoS_2, h-BN, and GaN Heterostructure. *ACS Nano* **2015**, *9*, 10032–10038.

10. Lopez-Sanchez, O.; Alarcon Llado, E.; Koman, V.; Fontcuberta i Morral, A.; Radenovic, A.; Kis, A. Light Generation and Harvesting in a van der Waals Heterostructure. *ACS Nano* **2014**, *8*, 3042–3048.

11. Kim, K.; Lee, T. H.; Santos, E. J. G.; Jo, P. S.; Salleo, A.; Nishi, Y.; Bao, Z. Structural and Electrical Investigation of C_{60}-Graphene Vertical Heterostructures. *ACS Nano* **2015**, *9*, 5922–5928.

12. Kim, K.; Santos, E. J. G.; Lee, T. H.; Nishi, Y.; Bao, Z. Epitaxially Grown Strained Pentacene Thin Film on Graphene Membrane. *Small* **2015**, *11*, 2037–2043.

13. Wang, Q. H.; Hersam, M. C. Room-temperature molecular-resolution characterization

of self-assembled organic monolayers on epitaxial graphene. *Nature Chem.* **2009**, *1*, 206–211.

14. Wang, Q. H.; Hersam, M. C. Nanofabrication of Heteromolecular Organic Nanostructures on Epitaxial Graphene via Room Temperature Feedback-Controlled Lithography. *Nano Lett.* **2011**, *11*, 589–593.

15. Cho, J.; Smerdon, J.; Gao, L.; Süzer, Ö.; Guest, J. R.; Guisinger, N. P. Structural and Electronic Decoupling of C_{60} from Epitaxial Graphene on SiC. *Nano Lett.* **2012**, *12*, 3018–3024.

16. Roy, S. S.; Bindl, D. J.; Arnold, M. S. Templating Highly Crystalline Organic Semiconductors Using Atomic Membranes of Graphene at the Anode/Organic Interface. *J. Phys. Chem. Lett.* **2012**, *3*, 873–878.

17. Zhang, L.; Roy, S. S.; Hamers, R. J.; Arnold, M. S.; Andrew, T. L. Molecular Orientation-Dependent Interfacial Energetics and Built-in Voltage Tuned by a Template Graphene Monolayer. *J. Phys. Chem. C* **2015**, *119*, 45–54.

18. Wang, C.; Dong, H.; Hu, W.; Liu, Y.; Zhu, D. Semiconducting π-Conjugated Systems in Field-Effect Transistors: A Material Odyssey of Organic Electronics. *Chem. Rev.* **2012**, *112*, 2208–2267.

19. Lee, T. H.; Kim, K.; Kim, G.; Park, H. J.; Scullion, D.; Shaw, L.; Kim, M.-G.; Gu, X.; Bae, W.-G.; Santos, E. J. G. et al. Chemical Vapor-Deposited Hexagonal Boron Nitride as a Scalable Template for High-Performance Organic Field-Effect Transistors. *Chem. Mater.* **2017**, *29*, 2341–2347.

20. Jariwala, D.; Howell, S. L.; Chen, K.-S.; Kang, J.; Sangwan, V. K.; Filippone, S. A.; Turrisi, R.; Marks, T. J.; Lauhon, L. J.; Hersam, M. C. Hybrid, Gate-Tunable, van der Waals p-n Heterojunctions from Pentacene and MoS_2. *Nano Lett.* **2016**, *16*, 497–503.

21. Bettis Homan, S.; Sangwan, V. K.; Balla, I.; Bergeron, H.; Weiss, E. A.; Hersam, M. C. Ultrafast Exciton Dissociation and Long-Lived Charge Separation in a Photovoltaic Pentacene-MoS_2 van der Waals Heterojunction. *Nano Lett.* **2017**, *17*, 164–169.

22. Briseno, A. L.; Mannsfeld, S. C. B.; Ling, M. M.; Liu, S.; Tseng, R. J.; Reese, C.; Roberts, M. E.; Yang, Y.; Wudl, F.; Bao, Z. Patterning organic single-crystal transistor arrays. *Nature* **2006**, *444*, 913–917.

23. Bao, Z.; Locklin, J. *Organic Field-Effect Transistors*; CRC Press, 2007.

24. Rogers, J. A.; Someya, T.; Huang, Y. Materials and Mechanics for Stretchable Electronics. *Science* **2010**, *327*, 1603–1607.

25. Fiori, G.; Bonaccorso, F.; Iannaccone, G.; Palacios, T.; Neumaier, D.; Seabaugh, A.; Banerjee, S. K.; Colombo, L. Electronics based on two-dimensional materials. *Nat. Nanotechnol.* **2014**, *9*, 768–779.

26. Krebs, F. C. Fabrication and processing of polymer solar cells: A review of printing and coating techniques. *Sol. Energ. Mat. Sol. Cells* **2009**, *93*, 394–412.

27. Yoo, S.; Domercq, B.; Kippelen, B. Efficient thin-film organic solar cells based on pentacene/C_{60} heterojunctions. *Appl. Phys. Lett.* **2004**, *85*, 5427–5429.

28. Parui, S.; Pietrobon, L.; Ciudad, D.; Vélez, S.; Sun, X.; Casanova, F.; Stoliar, P.; Hueso, L. E. Gate-Controlled Energy Barrier at a Graphene/Molecular Semiconductor Junction. *Adv. Func. Mater.* **2015**, *25*, 2972–2979.

29. Osada, K.; Tanaka, M.; Ohno, S.; Suzuki, T. Photoinduced charge transfer from vacuum-deposited molecules to single-layer transition metal dichalcogenides. *Jpn. J. Appl. Phys.* **2016**, *55*, 065201.

30. Jnawali, G.; Rao, Y.; Beck, J. H.; Petrone, N.; Kymissis, I.; Hone, J.; Heinz, T. F. Observation of Ground- and Excited-State Charge Transfer at the C_{60}/Graphene Interface. *ACS Nano* **2015**, *9*, 7175–7185.

31. Daughton, D. R.; Gupta, J. A. Orientation dependence of charge transfer for C_{60} on Cu(100). *Appl. Phys. Lett.* **2011**, *98*, 133303.

32. Gimzewski, J. K.; Modesti, S.; David, T.; Schlittler, R. R. Scanning tunneling microscopy of ordered C_{60} and C_{70} layers on Au(111), Cu(111), Ag(110), and Au(110) surfaces. *J. Vac. Sci. Technol., B* **1994**, *12*, 1942–1946.

33. Hashizume, T.; Motai, K.; Wang, X. D.; Shinohara, H.; Saito, Y.; Maruyama, Y.; Ohno, K.; Kawazoe, Y.; Nishina, Y.; Pickering, H. W. et al. Intramolecular structures of C_{60} molecules adsorbed on the Cu(111)-(1×1) surface. *Phys. Rev. Lett.* **1993**, *71*, 2959–2962.

34. Larsson, J. A.; Elliott, S. D.; Greer, J. C.; Repp, J.; Meyer, G.; Allenspach, R. Orientation of individual C_{60} molecules adsorbed on Cu(111): Low-temperature scanning tunneling microscopy and density functional calculations. *Phys. Rev. B* **2008**, *77*, 115434.

35. Altman, E. I.; Colton, R. J. Determination of the orientation of C_{60} adsorbed on Au(111) and Ag(111). *Phys. Rev. B* **1993**, *48*, 18244–18249.

36. Paßens, M.; Karthäuser, S. Interfacial and intermolecular interactions determining the rotational orientation of C_{60} adsorbed on Au(111). *Surf. Sci.* **2015**, *642*, 11–15.

37. Rogero, C.; Pascual, J. I.; Gómez-Herrero, J.; Baró, A. M. Resolution of site-specific bonding properties of C_{60} adsorbed on Au(111). *J. Chem. Phys.* **2002**, *116*, 832–836.

38. Rossel, F.; Pivetta, M.; Patthey, F.; Ćavar, E.; Seitsonen, A. P.; Schneider, W.-D. Growth and characterization of fullerene nanocrystals on NaCl/Au(111). *Phys. Rev. B* **2011**, *84*, 075426.

39. Tang, L.; Xie, Y.; Guo, Q. Complex orientational ordering of C_{60} molecules on Au(111). *J. Chem. Phys.* **2011**, *135*, 114702.

40. Wang, L.-L.; Cheng, H.-P. Density functional study of the adsorption of a C_{60} monolayer on Ag(111) and Au(111) surfaces. *Phys. Rev. B* **2004**, *69*, 165417.

41. Schull, G.; Berndt, R. Orientationally Ordered (7×7) Superstructure of C_{60} on Au(111). *Phys. Rev. Lett.* **2007**, *99*, 226105.

42. Tang, L.; Guo, Q. Orientational ordering of the second layer of C_{60} molecules on Au(111). *Phys. Chem. Chem. Phys.* **2012**, *14*, 3323–3328.

43. Zhou, H. T.; Mao, J. H.; Li, G.; Wang, Y. L.; Feng, X. L.; Du, S. X.; Müllen, K.; Gao, H.-J. Direct imaging of intrinsic molecular orbitals using two-dimensional, epitaxially-grown, nanostructured graphene for study of single molecule and interactions. *Appl. Phys. Lett.* **2011**, *99*, 153101.

44. Li, G.; Zhou, H. T.; Pan, L. D.; Zhang, Y.; Mao, J. H.; Zou, Q.; Guo, H. M.; Wang, Y. L.; Du, S. X.; Gao, H.-J. Self-assembly of C_{60} monolayer on epitaxially grown, nanostructured graphene on Ru(0001) surface. *Appl. Phys. Lett.* **2012**, *100*, 013304.

45. Švec, M.; Merino, P.; Dappe, Y. J.; González, C.; Abad, E.; Jelínek, P.; Martín-Gago, J. A. van der Waals interactions mediating the cohesion of fullerenes on graphene. *Phys. Rev. B* **2012**, *86*, 121407.

46. Jung, M.; Shin, D.; Sohn, S.-D.; Kwon, S.-Y.; Park, N.; Shin, H.-J. Atomically resolved orientational ordering of C_{60} molecules on epitaxial graphene on Cu(111). *Nanoscale* **2014**, *6*, 11835–11840.

47. Heiney, P. A. Structure, dynamics and ordering transition of solid C_{60}. *J. Phys. Chem. Solids* **1992**, *53*, 1333 – 1352.

48. David, W. I. F.; Ibberson, R. M.; Dennis, T. J. S.; Hare, J. P.; Prassides, K. Structural Phase Transitions in the Fullerene C_{60}. *Europhys. Lett.* **1992**, *18*, 219.

49. Li, G.; Zhou, H. T.; Pan, L. D.; Zhang, Y.; Mao, J. H.; Zou, Q.; Guo, H. M.; Wang, Y. L.; Du, S. X.; Gao, H.-J. Self-assembly of C_{60} monolayer on epitaxially grown, nanostructured graphene on Ru(0001) surface. *Appl. Phys. Lett.* **2012**, *100*, 013304.

50. Ovramenko, T.; Spillebout, F.; Bocquet, F. C.; Mayne, A. J.; Dujardin, G.; Sonnet, P.; Stauffer, L.; Ksari, Y.; Themlin, J. M. STM imagery and density functional calculations of C_{60} fullerene adsorption on the 6H-SiC(0001)-3×3 surface. *Phys. Rev. B* **2013**, *87*, 155421.

51. Chen, D.; Sarid, D. An STM study of C_{60} adsorption on Si(100)-(2 × 1) surfaces: from physisorption to chemisorption. *Surf. Sci.* **1995**, *329*, 206–218.

52. Pascual, J. I.; Gómez-Herrero, J.; Rogero, C.; Baró, A. M.; Sánchez-Portal, D.; Artacho, E.; Ordejón, P.; Soler, J. M. Seeing molecular orbitals. *Chem. Phys. Lett.* **2000**, *321*, 78–82.

53. Wang, H.; Zeng, C.; Wang, B.; Hou, J. G.; Li, Q.; Yang, J. Orientational configurations of the C_{60} molecules in the 2x2 superlattice on a solid $C_{60}(111)$ surface at low temperature. *Phys. Rev. B* **2001**, *63*, 085417.

54. Dresselhaus, M.; Dresselhaus, G.; Eklund, P. *Science of Fullerenes and Carbon Nanotubes*; Academic Press, 1996.

55. Leaf, J.; Stannard, A.; Jarvis, S. P.; Moriarty, P.; Dunn, J. L. A Combined Monte Carlo and Hückel Theory Simulation of Orientational Ordering in C_{60} Assemblies. *J. Phys. Chem. C* **2016**, *120*, 8139–8147.

56. Große, C.; Gunnarsson, O.; Merino, P.; Kuhnke, K.; Kern, K. Nanoscale Imaging of

Charge Carrier and Exciton Trapping at Structural Defects in Organic Semiconductors. *Nano Lett.* **2016**, *16*, 2084–2089, PMID: 26871739.

57. Clarke, T. M.; Durrant, J. R. Charge Photogeneration in Organic Solar Cells. *Chem. Rev.* **2010**, *110*, 6736–6767.

58. Santos, E. J. G.; Wang, W. L. Ultrafast charge-transfer in organic photovoltaic interfaces: geometrical and functionalization effects. *Nanoscale* **2016**, *8*, 15902–15910.

59. Hou, J. G.; Jinlong, Y.; Haiqian, W.; Qunxiang, L.; Changgan, Z.; Lanfeng, Y.; Bing, W.; Chen, D. M.; Qingshi, Z. Surface science: Topology of two-dimensional C_{60} domains. *Nature* **2001**, *409*, 304–305.

60. Sanchez-Sanchez, C.; Lanzilotto, V.; Gonzalez, C.; Verdini, A.; de Andres, P. L.; Floreano, L.; Lopez, M. F.; Martin-Gago, J. A. Weakly Interacting Molecular Layer of Spinning C_{60} Molecules on TiO_2(110) Surfaces. *Chem. Eur. J.* **2012**, *18*, 7382–7387.

61. Wang, Y.; Yamachika, R.; Wachowiak, A.; Grobis, M.; Crommie, M. F. Tuning fulleride electronic structure and molecular ordering via variable layer index. *Nature Mater.* **2008**, *7*, 194–197.

62. Chen, W.; Zhang, H.; Huang, H.; Chen, L.; Wee, A. T. S. Orientationally Ordered C_{60} on p-Sexiphenyl Nanostripes on Ag(111). *ACS Nano* **2008**, *2*, 693–698.

63. Altman, E. I.; Colton, R. J. Determination of the orientation of C_{60} adsorbed on Au(111) and Ag(111). *Phys. Rev. B* **1993**, *48*, 18244–18249.

64. Altman, E. I.; Colton, R. J. Nucleation, growth, and structure of fullerene films on Au(111). *Surf. Sci.* **1992**, *279*, 49–67.

65. Yuan, L.-F.; Yang, J.; Wang, H.; Zeng, C.; Li, Q.; Wang, B.; Hou, J. G.; Zhu, Q.; Chen, D. M. Low-Temperature Orientationally Ordered Structures of Two-Dimensional C_{60}. *J. Amer. Chem. Soc.* **2003**, *125*, 169–172.

516 66. Prato, M.; Lucchini, V.; Maggini, M.; Stimpfl, E.; Scorrano, G.; Eiermann, M.;
517 Suzuki, T.; Wudl, F. Energetic preference in 5,6 and 6,6 ring junction adducts of C_{60}:
518 fulleroids and methanofullerenes. *J. Amer. Chem. Soc.* **1993**, *115*, 8479–8480.

519 67. Porath, D.; Levi, Y.; Tarabiah, M.; Millo, O. Tunneling spectroscopy of isolated C_{60}
520 molecules in the presence of charging effects. *Phys. Rev. B* **1997**, *56*, 9829–9833.

521 68. Neças, D.; Klapetek, P. Gwyddion: an open-source software for SPM data analysis.
522 *Centr. Eur. J. Phys.* **2012**, *10*, 181–188.

523 69. Soler, J. M.; Artacho, E.; Gale, D., Julian; García, A.; Junquera, J.; Ordejón, P.;
524 Sánchez-Portal, D. The SIESTA method for ab initio order-N materials simulation. *J.*
525 *Phys. Condens. Matter* **2002**, *14*, 2745.

526 70. Kresse, G.; Hafner, J. *Ab initio* molecular dynamics for open-shell transition metals.
527 *Phys. Rev. B* **1993**, *48*, 13115–13118.

528 71. Kresse, G.; Furthmüller, J. Efficient iterative schemes for *ab initio* total-energy calcula-
529 tions using a plane-wave basis set. *Phys. Rev. B* **1996**, *54*, 11169–11186.

530 72. Perdew, J. P.; Burke, K.; Ernzerhof, M. Generalized Gradient Approximation Made
531 Simple. *Phys. Rev. Lett.* **1996**, *77*, 3865–3868.

532 73. Dion, M.; Rydberg, H.; Schröder, E.; Langreth, D. C.; Lundqvist, B. I. Van der Waals
533 Density Functional for General Geometries. *Phys. Rev. Lett.* **2004**, *92*, 246401.